Local energy flux of turbulent flows

Alexandros Alexakis*
Laboratoire de Physique de l'Ecole normale supérieure, ENS, Université PSL, CNRS, Sorbonne Université, Université de Paris, F-75005 Paris, France

Sergio Chibbaro†
Sorbonne Université, CNRS, UMR 7190, Institut Jean Le Rond d'Alembert, F-75005 Paris, France

(Received 4 May 2020; accepted 27 August 2020; published 18 September 2020)

We investigate the local energy flux rate $\Pi_\ell(\mathbf{x})$ towards small scales in isotropic turbulent flows using direct numerical simulations and applying different low-pass filters. Two different filters are examined: A sharp Fourier filter and a Gaussian filter. The probability density function (PDF) of the local energy flux is calculated for the different filters and for different filtering scales. It is shown that the local energy flux is a largely fluctuating quantity taking both negative and positive values and this is more pronounced for the sharp filter. The variance, skewness, and kurtosis of these fluctuations are shown to increase as the filtering scale is decreased. Furthermore, we calculate the joint PDF of $\Pi_\ell(\mathbf{x})$ with the local filtered strain rate S_ℓ and the enstrophy Ω_ℓ. The flux shows a good correlation with the strain, but not with the enstrophy. It is shown that its conditional mean value scales like $\langle\Pi_\ell\rangle_S \propto \ell^2 S_\ell^3$ in support of the Smagorinsky eddy viscosity model. Nonetheless, strong fluctuations exist around this value that also need to be modeled. We discuss the implications of our results for subgrid scale models and propose new modeling directions.

DOI: 10.1103/PhysRevFluids.5.094604

I. INTRODUCTION

Turbulent flows are the fundamental basis of many engineering applications [1,2], geophysics [3,4], and astrophysics [5], among others. To correctly capture the behavior of these complex problems with direct numerical simulation is, in principle, possible, but out of the question for the foreseeable time to come. This is because performing such simulations requires that all scales, from the largest (for instance, of the order of thousands of km for the atmosphere) to the smallest dissipative scales (of the order of cm for the atmosphere), need to be resolved. This leads to an enormous number of degrees of freedom whose evolution needs to be followed. In practice, a modeling approach is needed, where only the scales of interest are kept while the remaining scales are omitted and their effect on the former scales needs to be estimated. Because of the complexity of these flows, including complex geometry and several physical mechanisms at play, the most common way to arrive at such estimates is through semiempirical approaches [1,2,6]. In recent decades, an approach which has gained popularity is the large-eddy simulation (LES) [2,7–10]. In this framework, a low-pass filter is formally applied to equations, and only a part of the degrees of freedom (the large-scale motion) is directly solved, while the remaining scales are filtered out and their effect on the resolved scales is modeled by additional terms in the dynamical equations. Unfortunately, there is no separation of scales between large and small scales in turbulent flows

*alexakis@phys.ens.fr
†sergio.chibbaro@upmc.fr

to perform an asymptotic expansion, and therefore it is not possible to obtain a closed system of equations in a rigorous way [11–13]. It is therefore necessary to build up phenomenological closures based on our understanding of the physics of small-scale turbulence. Such phenomenological closures, however, need to be thoroughly tested with real data. For this goal, direct numerical simulations (DNS) appear as the most valuable tool to get insights that permit the assessment of present models and their improvement [2,14–16]

For any such modeling attempt, it is key to find a good compromise between including an accurate physics and keeping the structure of the model simple and computationally efficient. With this in mind, in this work we have focused on the analysis of the most important element in turbulence dynamics, that is, the energy flux underlying the cascade [17]. The principal aim of the present work is thus to get physical insights into the cascade process with regard to the multiscale character of turbulent flows.

We investigate, therefore, how the transfer of energy to the subgrid scales can be modeled and what observable of the resolved scales it should be based on. In order to address this question, we perform a high-resolution numerical simulation and apply a scale-by-scale analysis based on the original approach by Germano [7]. This allows us to simultaneously measure the effect of the small filtered scales on the unfiltered scales, as in [18–22], but at the same time to associate it with different observables of the large scales. To identify such observables, we look at the gradients of the flow that have been useful in giving insights into the cascade mechanisms [13,23,24]. A similar approach was used in the important work by Borue and Orszag [18] at low Reynolds number, where many insights are already given.

More specifically, in this work we report on a comprehensive analysis of the flux in relation to the total strain and vorticity. This is achieved by calculating the probability density function (PDF) of the local energy flux for different filters and for different filtering scales as well as the joint PDF of the flux with two observables, i.e., the strain and enstrophy of the filtered flow. This allows us to extract correlations between the flux and the two observables. Our results strongly support the use of the Smagorinsky model [25], but also emphasizes its drawbacks. We conclude by discussing the implications of our results to modeling and also propose a possible new subgrid scale model.

II. THEORETIC BACKGROUND

A. Definitions

We begin by considering the incompressible Navier-Stokes equations describing the evolution of the velocity field $\mathbf{u}$ of an incompressible unit density fluid given by

$$\frac{\partial \mathbf{u}}{\partial t} + \mathbf{u}\cdot\nabla\mathbf{u} = -\nabla p + \nu\nabla^2\,\mathbf{u} + \mathbf{f}, \tag{1}$$

$$\nabla\cdot\mathbf{u} = 0, \tag{2}$$

where p is the pressure, ν is the viscosity, and $\mathbf{f}$ is an external body force. The flow is contained in a cube of side 2π and periodic boundary conditions are assumed.

To introduce the notion of different scales in the flow, we use a filtering or coarse-graining approach [7], where the dynamic velocity field $\mathbf{u}$ is spatially (low-pass) filtered over a scale ℓ to obtained a filtered value $\overline{\mathbf{u}}_\ell(\mathbf{x})$. The filtering procedure is given by

$$\overline{\mathbf{u}}_\ell(\mathbf{x}) = \int d^3r\, G_\ell(\mathbf{r})\mathbf{u}(\mathbf{x}+\mathbf{r}), \tag{3}$$

where G_ℓ is a smooth filtering function, spatially localized and such that $G_\ell(\vec{r}) = \ell^{-3}G(\vec{r}/\ell)$, where the function G satisfies $\int d\vec{r}\; G(\vec{r}) = 1$, and $\int d\vec{r}\; |\vec{r}|^2 G(\vec{r}) = O(1)$. By applying the filtering to Navier-Stokes equations, we obtain the coarse-grained dynamics,

$$\partial_t\overline{\mathbf{u}}_\ell + (\overline{\mathbf{u}}_\ell\cdot\nabla)\overline{\mathbf{u}}_\ell = -\nabla\overline{p}_\ell - \nabla\cdot\boldsymbol{\tau}_\ell + \nu\nabla^2\overline{\mathbf{u}}_\ell. \tag{4}$$

Here, $\boldsymbol{\tau}_\ell$ is the *subscale stress tensor* (or momentum flux) which describes the force exerted on scales larger than ℓ by fluctuations at scales smaller than ℓ. It is given by

$$(\boldsymbol{\tau}_\ell)_{i,j} = \overline{(u_i u_j)}_\ell - (\overline{u}_\ell)_i (\overline{u}_\ell)_j. \tag{5}$$

The corresponding pointwise kinetic energy budget reads

$$\partial_t\left(\tfrac{1}{2}|\overline{\mathbf{u}}|^2\right) + \partial_j\left[\left(\tfrac{1}{2}|\overline{\mathbf{u}}|^2 + \overline{p}\right)\overline{u}_j + \tau_{ij}\overline{u}_i - \nu\partial_j\left(\tfrac{1}{2}|\overline{\mathbf{u}}|^2\right)\right] = -\Pi_\ell - \nu|\boldsymbol{\nabla}\overline{\mathbf{u}}|^2, \tag{6}$$

where we have dropped the ℓ subscript whenever unambiguous for the sake of clarity, and

$$\Pi_\ell(\mathbf{x}) \equiv -(\partial_j\overline{u}_i)\tau_{ij} \tag{7}$$

is the subgrid scale (SGS) energy flux. This term is key since it represents the space-local transfer of energy among large and small scales across the scale ℓ. In the case of a direct energy cascade, the flux is known to be positive on average.

Although we formulate our filtering procedure in the physical space, in homogeneous flows an efficient way to implement the filter is to use its Fourier transform,

$$\hat{G}_q(\mathbf{k}) = \int G_\ell(\mathbf{x}) e^{i\mathbf{k}\cdot\mathbf{x}} d\mathbf{x}, \tag{8}$$

where $q = 1/\ell$ is the filtering wave number. In this work, we consider two types of filters. First we consider a Gaussian kernel,

$$\hat{G}_q(\mathbf{k}) = \exp\left[-\frac{k^2}{2q^2}\right]. \tag{9}$$

For an infinite domain, this filter corresponds to the Gaussian filter in real space, $G_\ell(r) = \exp(-\frac{1}{2}r^2/\ell^2)/(2\pi\ell^2)^{3/2}$. We note that this filtering is not a projection and, in general, $\overline{(\overline{\mathbf{u}}_\ell)}_\ell \neq \overline{\mathbf{u}}_\ell$. The second filter we are going to use is a sharp-spectral filter such that

$$\overline{\mathbf{u}}_\ell(\mathbf{x}, t) = \sum_{|\mathbf{k}|<q} \hat{\mathbf{u}}(\mathbf{k}, t) e^{i\mathbf{k}\cdot\mathbf{x}}. \tag{10}$$

This filtering is a projector ($\overline{(\overline{\mathbf{u}}_\ell)}_\ell = \overline{\mathbf{u}}_\ell$) and is based on a Galerkin truncation for all wave numbers larger than the given cutoff $q = 1/\ell$. This filtering is related to the classical definition of the energy flux $\Pi(q)$ given by

$$\Pi(q) = \langle \overline{\mathbf{u}}_\ell(\mathbf{u}\cdot\boldsymbol{\nabla})\mathbf{u}\rangle, \tag{11}$$

where the angular brackets stand for spatial average and Eq. (10) has been used for $\overline{\mathbf{u}}_\ell$. Furthermore, when the sharp filtering is used, the relation

$$\langle \Pi_\ell(\mathbf{x})\rangle = \Pi(q) \tag{12}$$

holds.

B. Modeling

Given that in a LES only scales larger than ℓ are resolved, it is desirable to model the subscale stress tensor $\boldsymbol{\tau}_{i,j}$ based on the resolved scales and their geometric structure so that a closed system of equations is obtained. The simplest choice is to relate $\boldsymbol{\tau}_{i,j}$ to the velocity gradient tensor of the filtered field $\boldsymbol{\nabla}\overline{\mathbf{u}}_\ell$. It can be decomposed into its symmetric and antisymmetric parts as $\boldsymbol{\nabla}\overline{\mathbf{u}}_\ell = \overline{\mathbf{S}}_\ell + \overline{\boldsymbol{\Omega}}_\ell$, with

$$\overline{\mathbf{S}}_\ell = \left(\boldsymbol{\nabla}\overline{\mathbf{u}}_\ell + \boldsymbol{\nabla}\overline{\mathbf{u}}_\ell^T\right)/2 \quad \text{and} \quad \overline{\boldsymbol{\Omega}}_\ell = \left(\boldsymbol{\nabla}\overline{\mathbf{u}}_\ell - \boldsymbol{\nabla}\overline{\mathbf{u}}_\ell^T\right)/2. \tag{13}$$

The symmetric part is related to the strain, whereas the antisymmetric part is related to the vorticity. It is worth recalling that these quantities are related on average, $\langle|\overline{\mathbf{S}}_\ell|^2\rangle = \langle|\overline{\boldsymbol{\Omega}}_\ell|^2\rangle$ [12], but the local

properties are not. Using these tensors, the subscale energy flux is defined as $\Pi_\ell = \overline{\mathbf{S}}_\ell : \boldsymbol{\tau}_\ell$, so that it is clear that only the symmetric part of the resolved gradients enters directly in the definition of the flux. Yet, the dependence of the subscale stress $\boldsymbol{\tau}$ on the strain and vorticity is not known *a priori*.

Several attempts to model the subscale stress tensor by $\overline{\mathbf{S}}_\ell$ and $\overline{\boldsymbol{\Omega}}_\ell$ have been made [2,9]. The simplest models use the norms of the tensors, $S_\ell^2 = |\overline{\mathbf{S}}_\ell|^2$ and $\Omega_\ell^2 = |\overline{\boldsymbol{\Omega}}_\ell|^2$. From these, the most popular model is given by the Smagorinsky model [25] where $\boldsymbol{\tau}$ is modeled as

$$\boldsymbol{\tau}_{i,j} \approx -C_s^2 \ell^2 S_\ell \overline{\mathbf{S}}_{i,j}, \tag{14}$$

where C_s is an order one nondimensional number and we use the symbol $\approx$ to indicate that the relation above is a model and is not an exact result. This expression gives the following estimate for the local energy flux:

$$\Pi_\ell \approx C_s^2 \ell^2 S_\ell^3. \tag{15}$$

Other models take into account $\overline{\boldsymbol{\Omega}}_\ell$ as well. Indeed, approximating the subscale stress with its extreme local expression, which is as a function of the resolved scale, the nonlinear Clark model is obtained [9],

$$\tau_\ell(\mathbf{u},\mathbf{u}) \approx \tfrac{1}{3} C_2 \ell^2 \big(\overline{\mathbf{S}}_\ell^2 + \overline{\boldsymbol{\Omega}}_\ell^2 + \overline{\boldsymbol{\Omega}}_\ell \overline{\mathbf{S}}_\ell - \overline{\mathbf{S}}_\ell \overline{\boldsymbol{\Omega}}_\ell\big), \tag{16}$$

where both strain and vorticity participate in the dynamics [18,26]. For this model, the formula for the flux is

$$\Pi_\ell \approx \tfrac{1}{3} C_2 \ell^2 \big[-\mathrm{Tr}\big(\overline{\mathbf{S}}_\ell^3\big) + 3\mathrm{Tr}\big(\overline{\mathbf{S}}_\ell \overline{\boldsymbol{\Omega}}_\ell^2\big)\big], \tag{17}$$

which shows that the local behavior of the flux depends on a term related to pure strain and on the term linked to vortex stretching [13]. Generally speaking, the *local* dynamics of strain and vortex stretching can be quite independent [27], and therefore a complete picture of the cascade requires both. Nonetheless, it is well known that for a homogeneous average, there is the following kinematic relation [28]: $\langle -\mathrm{Tr}(\overline{\mathbf{S}}_\ell^3)\rangle = \langle 9\mathrm{Tr}(\overline{\mathbf{S}}_\ell \overline{\boldsymbol{\Omega}}_\ell^2)\rangle$, such that the mean flux can be related to the sole vortex-stretching term (or the strain skewness). Furthermore, the similarity of the statistics of these two terms was observed previously in a different context [29]. This suggests that within the purpose of modeling the cascade flux, the use of the sole strain may be justified. Nonetheless, all mentioned models are based on assumptions that cannot be proven from basic principles. Therefore, confirmation from numerical simulations and experiments is required. One thus has to compare the results of direct numerical simulations (DNS) with different LES models [9,30] or, alternatively, one can use DNS to directly test the assumptions used by the models, i.e., the *a priori* approach [10]. This latter choice is what we are trying to do in the following sections.

III. RESULTS

A. The flow

We apply the formalism described in the previous section to the results of a direct numerical simulation of the Navier-Stokes equations given by Eq. (2). The forcing was chosen so that there is a constant injection of energy at the Fourier modes with $|\mathbf{k}| \leqslant \mathbf{k_f} = \mathbf{2}$ and is explicitly given in terms of its Fourier components as

$$\hat{\mathbf{f}}_\mathbf{k} = \epsilon \sum_{|\mathbf{k}|\leqslant \mathbf{2}} \frac{\hat{\mathbf{u}}_\mathbf{k}}{\sum_{|\mathbf{k}|\leqslant 2} |\hat{\mathbf{u}}_\mathbf{k}|^2} + i \sum_{|\mathbf{k}|\leqslant 2} \omega_\mathbf{k} \hat{\mathbf{u}}_\mathbf{k}, \tag{18}$$

where ϵ is the constant in time energy injection rate that we fix to $\epsilon = 1$. The frequencies $\omega_\mathbf{k}$ are chosen randomly in order to decorrelate the forced modes. The flow was simulated using the pseudospectral open-source code GHOST [31] with a second-order Runge-Kutta for time advancement and using the 2/3 rule for removing de-aliasing errors. The code has been extensively validated

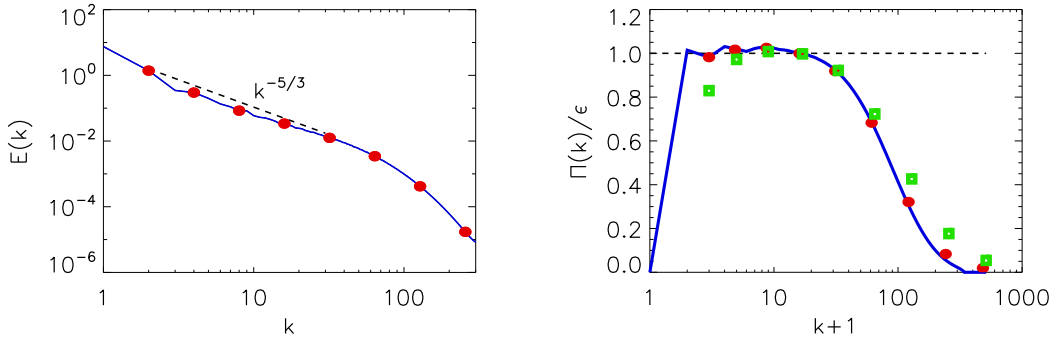

FIG. 1. Left: Energy spectrum for the simulation that is analyzed. The forcing is at $k_f = 1$. A dashed line with slope $-5/3$ is added for reference. The red dots indicate the wave numbers at which the filtering was applied in the following sections. Right: Average energy flux $\langle \Pi_\ell \rangle$ normalized with the mean rate of dissipation obtained without filtering (DNS) and with the sharp filter (red dots) and the Gaussian filter (green squares).

during the last two decades and is a reference for homogeneous turbulence [31]. The simulations were carried out with $\nu = 0.0005$ on a 1024^3 grid leading in each direction to a maximum wave number $k_{\max} = N/3 \simeq 341$. The Reynolds number $\mathrm{Re} = \epsilon^{1/3} k_1^{-4/3}/\nu$ achieved with this resolution was $\mathrm{Re} = 2000$, where $k_1 = 1$ is the smallest nonzero wave number in the domain. After a short transient, the flow reaches a steady state where the energy dissipation rate matches the energy injection rate and the flow shows all characteristics of a classical isotropic turbulent flow. In Fig. 1, we show the energy spectrum defined as

$$E(k) = \frac{1}{2} \sum_{k-1<|\mathbf{q}|\leqslant k} |\hat{\mathbf{u}}_q|^2,$$

where $\hat{\mathbf{u}}_q$ is the velocity Fourier mode. The spectrum shows a standard behavior, with a reasonable inertial range following a Kolmogorov power-law scaling $E(k) \propto k^{-5/3}$ until around $k = 50$. The red dots indicate the wave numbers where filtering was applied, which is examined in the next sections. In the right panel, we show the energy flux that is almost constant in the inertial range. The flux marked by a solid line was calculated directly in Fourier space as is typically done in pseudospectral codes using Eq. (11). The red circles indicate the space averaged local flux for the sharp filter of Eq. (10) at the different filtering wave numbers q, which are going to be examined in the remaining sections of this work. With green squares, the space averaged local flux for the Gaussian filter of Eq. (9) is also shown for the same wave numbers. As expected, the sharp projector perfectly overlaps on the solid line, while the mean energy flux obtained from the Gaussian filter does not exactly match, notably at small scales [32]. The two results are considerably close, however, in the inertial range. We now consider the qualitative phenomenology of the flow as represented through filtering at different scales. In Fig. 2, we show the vorticity field at different coarse-graining levels using the Gaussian filter. The filtering at different scales reveals a hierarchy of vortices of different scales coexisting in the flow. The unfiltered field shows small vortex filaments typical of isotropic turbulence. When filtered at small scales $q = 64$ and also at an inertial scale, the field shows some qualitative self-similarity even though the smallest filaments are smoothed out. As the filtering wave number is reduced, larger and large vortices are revealed. Even when most of the scales are filtered out, $q = 16$, some residual elongated vortex tubes persist, pointing out the most important spatial, yet temporally intermittent, coherent structures of the flow.

B. PDF of local fluxes

Using the flow described in the previous section, we calculate the local energy flux $\Pi_\ell(\mathbf{x})$ of Eq. (3) at different levels of filtering $q = 1/\ell$ using both the Gaussian and the sharp filter and

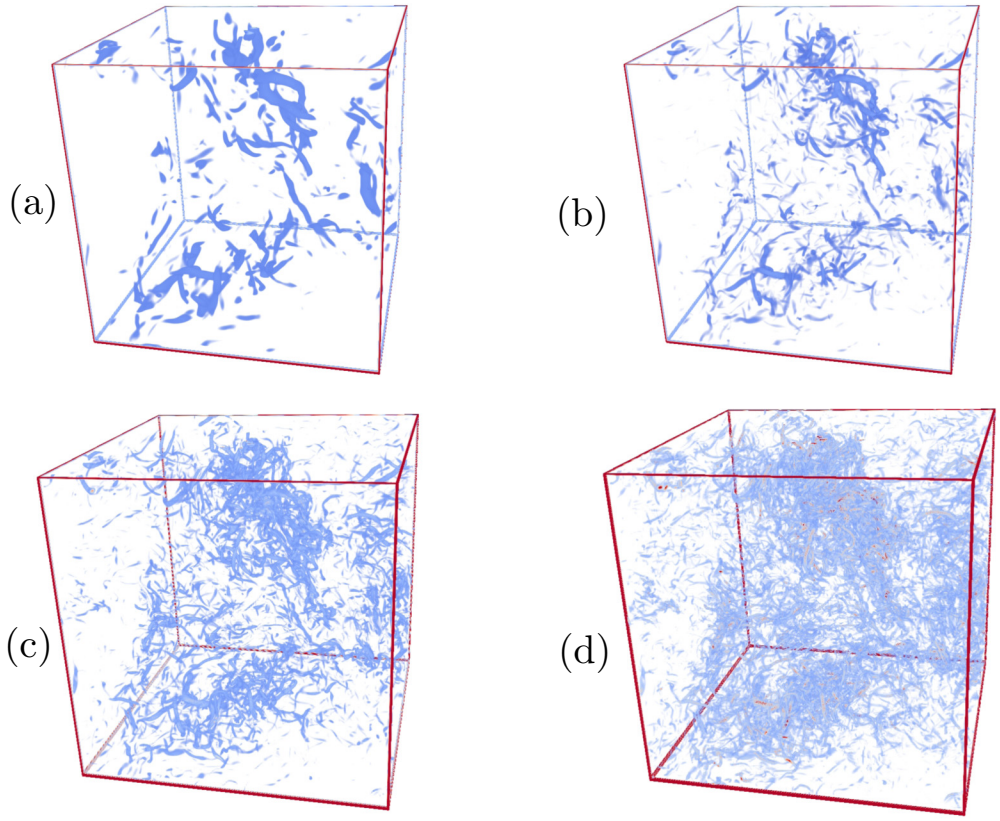

FIG. 2. The enstrophy of the filtered field for (a) $q = 16$, (b) $q = 32$, and (c) $q = 64$, using the Gaussian filter, and (d) unfiltered. The threshold used for the visualization is 3σ.

analyze its statistical properties. The local flux was calculated for q equal to powers of 2, $q = 2^n$, where n ranges from 1 to 8, as indicated in Fig. 1. This calculation was repeated for several instances of time so that we obtained a good statistical sample. In Fig. 3, we show the PDFs of Π_ℓ at different scales, from the large ($q = 8$) to the small ($q = 256$) scales. For both filters, the PDFs are centered

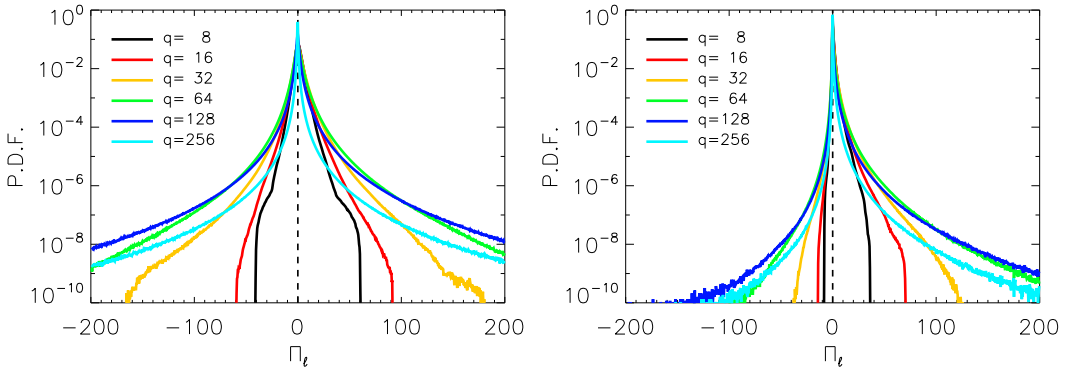

FIG. 3. The PDFs of the subscale energy flux for the sharp filter (left) and for the Gaussian filter (right). The PDFs are displayed for different length-scale cutoff ℓ.

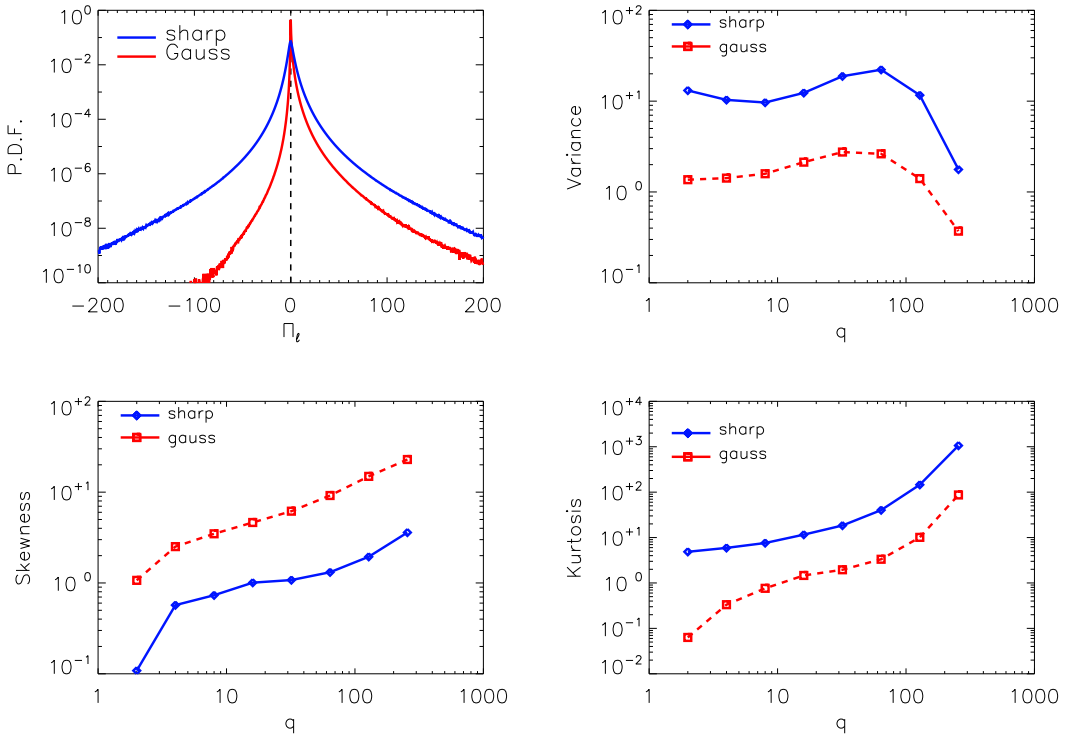

FIG. 4. Top left panel: A comparison of the PDF of the flux using the sharp filter (blue line) and a Gaussian filter (red line) for $q = 64$. Top right panel: The variance of the flux as a function of q for the two filters. Bottom panels: The skewness (left) and the flatness (right) of the flux for the two filters.

around a value close to zero with long exponential or stretched exponential tails. The tails of the PDF increase as q is increased up until the dissipation scales are reached, $q \simeq 128$, after which they start to decrease. It is worth noting that for $q > k_{\max}$, the local flux is pointwise zero so the PDF converges to a δ function at $\Pi_\ell(x) = 0$.

The flux obtained by sharp filtering is more symmetric and displays larger tails. The flux obtained through Gaussian filtering has a more skewed behavior, with less probable negative events. The profiles obtained are similar to those obtained in analogous previous simulations [20,32,33]. In the top right panel of Fig. 4, we compare the two fluxes based on the two filters at the scale $\ell = 1/q = 1/64$, which is at the end of the inertial range and emphasizes the differences of the PDFs of the two filters. In the rest of the panels of Fig. 4, we show the first normalized statistical moments of the flux:

$$\text{the variance} \quad \langle [\Pi_\ell - \langle \Pi_\ell \rangle]^2 \rangle, \tag{19}$$

$$\text{the skewness} \quad \frac{\langle [\Pi_\ell - \langle \Pi_\ell \rangle]^3 \rangle}{\langle [\Pi_\ell - \langle \Pi_\ell \rangle]^2 \rangle^{3/2}}, \quad \text{and the kurtosis} \quad \frac{\langle [\Pi_\ell - \langle \Pi_\ell \rangle]^4 \rangle}{\langle [\Pi_\ell - \langle \Pi_\ell \rangle]^2 \rangle^2}, \tag{20}$$

computed at different scales and for the two filters. Here we have a vivid description of the difference between the two results. The flux computed through the Gaussian filter at this scale is characterized by strong fluctuations, with possible but rare negative events. It is interesting to point out that the shape exhibited by the one-point PDF of the flux shown in Fig. 4 is qualitatively the same as those found in the study of general dissipative nonequilibrium systems, in the framework of the Gallavotti-Cohen or fluctuation-relation analysis [34–42]. Instead, the negative events (or backscatter events, as

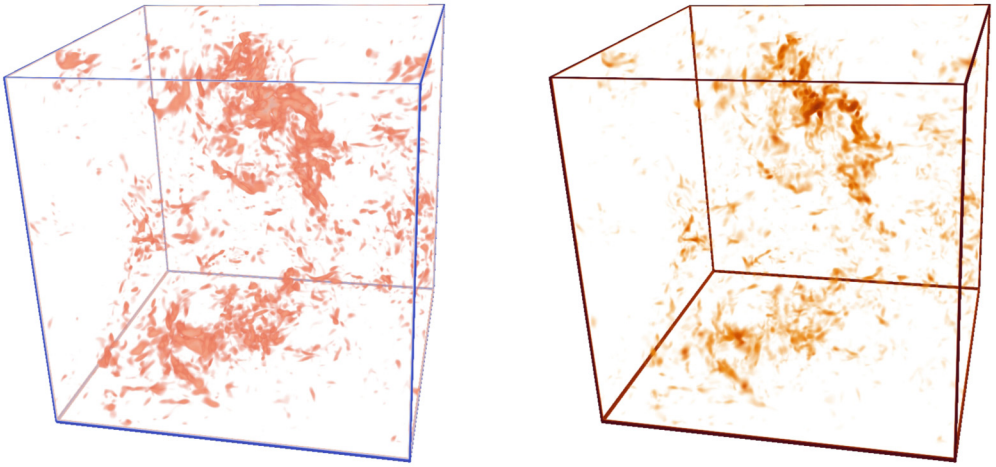

FIG. 5. A visualization of the strain density (left) and the amplitude of the local flux (right), for $q = 32$ and gauss filtering (for the same snapshot of the flow as in Fig. 2).

called in LES) are much more frequent with the sharp filter. It is interesting to look at the statistical moments, which show that the two approaches give the same trend up to the fourth moment at all scales, within the numerical errors, but there is about one order of magnitude of difference between the two results almost everywhere. While the average flux is the same computed by the two different methods, the sharp filter gives a wildly fluctuating subscale energy flux, with many negative events, so that it appears difficult to use directly in the framework of LES, at least from a numerical point of view. The reason for such discrepancy is traced back to the fact that the sharp filter used here does not have the desirable features of a proper filter; notably, it is not localized in space and is not positive definite. Even though it has been shown that the sharp-spectral filter has a firm theoretical basis for its use in LES, the results suggest that the use of the smooth filtering approach is preferable if one is interested in energy flux properties. For this reason, we focus in the following on the Gaussian filter.

C. Joint PDF

We now look at the possible dependence of the local energy flux with the gradients of the flow as discussed in Sec. II B. To give some more visual insight, in Fig. 5 we show a three-dimensional visualization of the coarse-grained strain S_ℓ and the energy flux Π_ℓ at the same scale, side by side. We have chosen a moderately large scale, $q = 32$, since at these scales the dependence on vorticity seems more important. The figure convincingly shows that most of the properties of the flux and, notably, the geometrical features are well reproduced by the strain. In particular, Π_ℓ appears to be more correlated with the filtered strain than the filtered enstrophy shown in the top right panel of Fig. 2 for the same q.

To be more quantitative, we calculate the joint PDF between Π_ℓ and Ω_ℓ^2 and between Π_ℓ and S_ℓ^2. The strain and the enstrophy are multiplied with the viscosity to be able to compare with the mean value at $\ell = 0$ given by

$$\lim_{\ell\to 0} \nu\langle S_\ell^2\rangle = \lim_{\ell\to 0} \nu\langle \Omega_\ell^2\rangle = \epsilon = 1.$$

The results are displayed in Fig. 6. From the left column, we can see that the energy flux is essentially uncorrelated with the enstrophy, and therefore with vorticity. In particular, for large q, we observe that at a given Π_ℓ, the probability changes very slowly with respect to Ω, indicating almost independence. The joint PDF of the flux with the strain presents a very different story. The

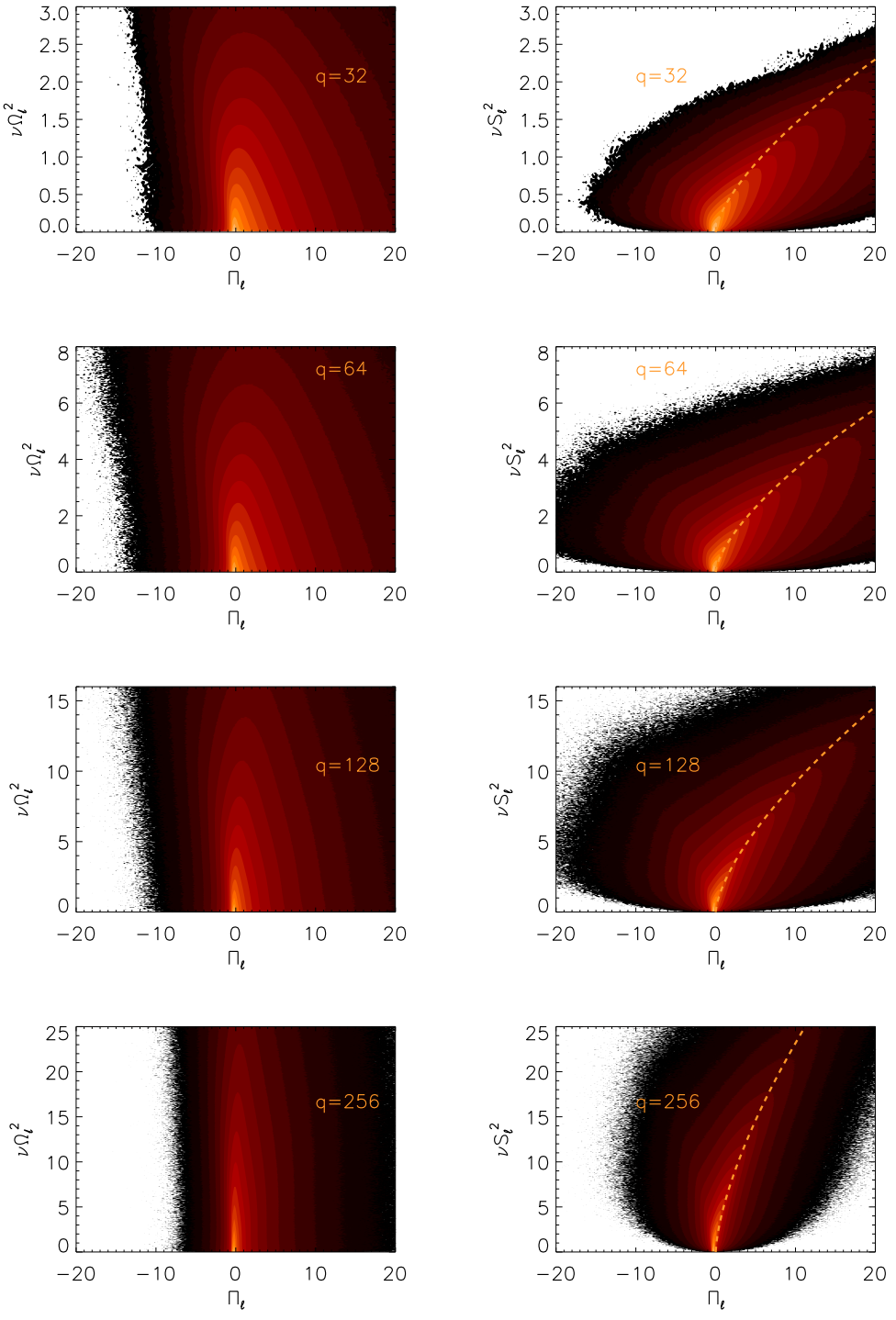

FIG. 6. Left column: Joint PDF of flux Π_ℓ and enstrophy Ω^2 at different scales. Right column: Joint PDF of flux Π_ℓ and strain S^2 at different scales. Bright colors indicate high probability, while dark colors indicate low probability; white indicates zero probability. The strain and the enstrophy are multiplied with the viscosity to be able to compare with the mean value at $\ell = 0$ given by $\nu\langle S^2\rangle = \nu\langle\Omega^2\rangle = \epsilon = 1$.

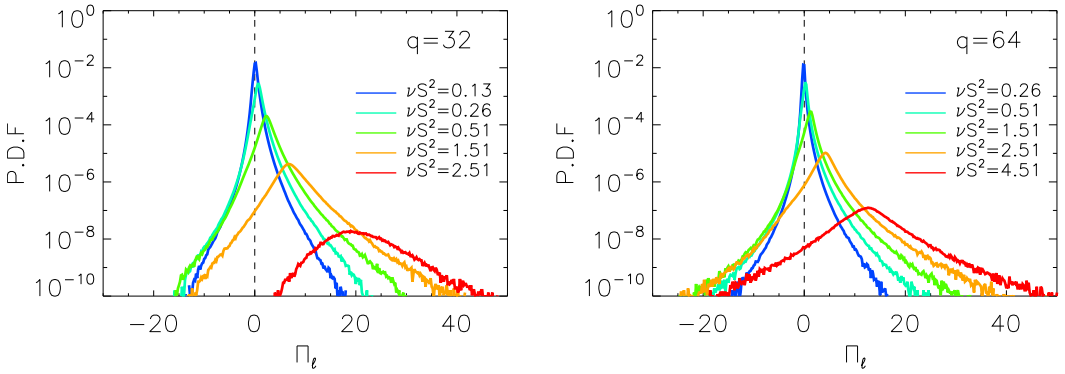

FIG. 7. The PDF of the flux conditioned on different values of the strain S_ℓ for $q = 32$ (left) and $q = 64$ (right).

two variables appear very strongly correlated at each scale. Furthermore, even though the change of scale has an impact on the shape of the PDF, it appears to change in a self-similar way, that is, the dependence on the scale is given by a power law. To quantitatively capture this trend, we show in all figures the curve given by the Smagorinsky model (15). The agreement of this curve with the maximum of the probability is excellent. Qualitatively, regions with high strain favor large energy flux. Furthermore, as expected, the larger the scales, the less important the strain can be, so that very large strain values are obtained at very small scales, where they contribute to the viscous dissipation. It is worth noting that the variations around the maximum value [given approximately by Eq. (15)] are significant and Π_ℓ also takes negative values. This is most significant for small values of S, while for large values of S, the flux is almost always positive. To get more insights on the behavior of the fluctuations, we plot the shape of the PDF of the subscale flux Π_ℓ at a given scale conditioned with several values of the strain, shown in Fig. 7 for the scale $\ell = 1/q = 1/32$ and $\ell = 1/64$. While the mean value and the maximum follow the S_ℓ^3 curve, the shape of the curves changes even at the qualitative level. Indeed, positive extreme events are found only for large strains, which means more pronounced right tails for the corresponding PDFs. Although the analysis focuses on rare events and therefore statistical errors may lead to wrong conclusions, it is interesting to make the following remarks: (i) The negative side of the flux is less affected by changes in S_ℓ^2, at small values of the strain. (ii) However, as larger values of S_ℓ^2 are examined, less negative events are observed, notably at the larger scale shown, $q = 32$. Thus, large strain regions are related dominantly to positive flux. (iii) At different scales, the fluctuations of the flux display a different behavior, in particular when conditioned on a high value of the strain.

Furthermore, to examine the dependence on scales, as highlighted in Fig. 6, we have analysed the self-similarity of the behavior and the results are displayed in Fig. 8. The left panel shows as a function of νS_ℓ^2, the mean value of the flux conditioned on the strain $\langle \Pi_\ell \rangle_S$, where the average is performed over all points that have a given strain S_ℓ. The curves nicely collapse, pointing out the behavior indicated by Eq. (15). The results of the mean value thus suggest that the mean flux can be estimated and thus modeled by the value of the strain rate following the relation (15). However, in addition to the mean value, a successful model should also capture the fluctuations around it. This is particularly important in this case since, as shown in Fig. 7, although $\langle \Pi_\ell \rangle_S$ is always positive, the fluctuations are strong enough that Π_ℓ also takes negative values.

To see if a similar relation is followed by the fluctuations and to look for a possible self-similar behavior of the fluctuations, we plot the variance of the conditioned Π_ℓ in the left panel of Fig. 8. The behavior of the variance is not fully self-similar, as already pointed out in Fig. 7. As q is varied, different slopes are observed. For scales in the inertial range and larger $q \leqslant 64$, the slope observed in the left panel of Fig. 8 (indicating a possible power-law dependence) is decreasing with

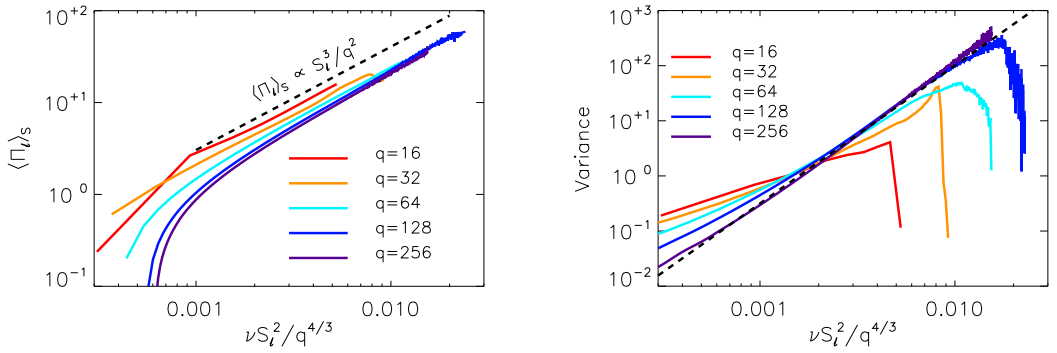

FIG. 8. Left: The mean conditioned flux $\langle\Pi_\ell\rangle_S$ as a function S_ℓ. Right: The variance of the conditioned flux as a function of S_ℓ.

q. Only in the dissipative range, $q > 64$, do the curves almost collapse. This lack of self-similarity is a clear sign of intermittency that currently lacks a theoretical understanding and requires further investigation.

IV. DISCUSSION

The main focus of the present multiscale analysis of the cascade energy process is to give some fundamental insights into the relation to LES of turbulent flows, where only scales larger than ℓ are simulated and their effect of the subfilter scales has to be modeled. First, our results show that while the sharp-spectral filter has been shown to fulfill the needed mathematical properties [32,43–46] and is the most obvious filter for pseudospectral simulations, it triggers wild fluctuations that blur the cascade-flux process and make it difficult to understand its main properties. That seems related to the fact that most of the quantities under investigation are found to be local in space, and hence our findings suggest a preference for the use of filters which are local and positive in physical space.

Then, our scale-by-scale analysis shows that there is a strong correlation between the local energy flux rate and strain rate of the filtered field. The conditional mean value of the flux rate follows a clear power-law dependence on the strain rate given by Eq. (15), making it predictable based on only filtered quantities. Thus the strain is a very good observable to characterize the properties of the energy flux. On the other hand, the vorticity appears to be much more indirectly linked. The scaling relation observed in this work hence gives strong support to the Smagorinsky model and its variants [2,25] that use the strain to predict the subscale stress tensor. However, even though the Smagorinsky model predicts to good accuracy the mean values, it gives no prediction for the fluctuations around the mean that are of great importance as they control the inverse transfer events that are observed.

There are several steps that can be taken to extend this research. First of all, simulations at higher Reynolds number would be desirable in order to have a cleaner inertial range where the statistics are not affected either by the forcing properties or from viscous effects. Second, the present results were limited in considering correlations of the local flux with only the amplitude of the strain and the vorticity. This is a simplification that is required as a first step before examining more complex relations as the one given by the Clark model (16). It was also noted that although the vorticity was not strongly correlating with the flux, it was not completely disassociated from it. So a relation that involves both strain and vorticity is still a possible improvement of the Smagorinsky model. A fruitful direction that could be followed in future work is to examine the joint PDF of the energy flux and the invariants (under rotations and reflections) of the gradient tensor [47,48] that completely characterize the structure of the gradient tensor. Third, it would be important, of course, to extend

such an analysis to bounded flows, for instance a channel, which is key for applications and where the local inverse cascade is important.

Furthermore, even if an optimal parametrization is chosen, the energy flux will still depend on the subscale fluctuations that are essentially random in nature. One cannot then hope to get an exact relation that connects the gradient tensor with the flux, and this randomness will need to be taken into account in terms of stochastic modeling. In terms of the Smagorinsky model, the simplest expression that generalizes Eq. (14) can be given by

$$\boldsymbol{\tau}_{i,j} \approx -C_s^2 \ell^2 S_\ell (1 + \xi_\ell) \overline{\mathbf{S}}_{i,j}, \tag{21}$$

where ξ_ℓ is a zero mean spatiotemporal noise that depends, in principle, on ℓ and S_ℓ and whose properties need to be determined from data. Analyzing the data displayed in Fig. 7, it turns out that it is not possible to fit all the curves with a simple random variable ξ since nontrivial dependence of ℓ and S_ℓ is indeed found. Yet, the main features are decently recovered simply with a random variable whose PDF is given by $f(x) \propto \exp(-\gamma_S |x|)$, where γ_S is a coefficient that has a dependence on S. Finally, besides the energy, the cascade of the second invariant, i.e., that of helicity, also needs to be studied, quantified, and properly modeled. We plan to follow these directions in our future work.

ACKNOWLEDGMENTS

This work was granted access to the HPC resources of MesoPSL financed by the Région Ile de France and the project Equip@Meso (Ref. No. ANR-10-EQPX-29-01) of the program Investissements d'Avenir supervised by the Agence Nationale pour la Recherche and the HPC resources of TGCC-CURIE and CINESOccigen (Allocations No. A0070506421 and No. A0062B10759) attributed by GENCI (Grand Equipement National de Calcul Intensif), where the present numerical simulations were performed. This work was also supported by the Agence Nationale de la Recherche (ANR DYSTURB Project No. ANR-17-CE30-0004).

[1] A. S. Monin and A. M. Yaglom, *Statistical Fluid Mechanics* (MIT Press, Cambridge, MA, 1975).
[2] S. B. Pope, *Turbulent Flows* (Cambridge University Press, Cambridge, 2000).
[3] A. E. Gill, *Atmosphere-ocean Dynamics* (Elsevier, New York, 2016).
[4] S. A. Thorpe *et al.*, *An Introduction to Ocean Turbulence* (Cambridge University Press, Cambridge, 2007), Vol. 10.
[5] D. Biskamp, *Magnetohydrodynamic Turbulence* (Cambridge University Press, Cambridge, 2003).
[6] D. C. Wilcox, *Turbulence Modeling for CFD* (DCW Industries, La Canada, CA, 1998), Vol. 2.
[7] M. Germano, Turbulence: The filtering approach, J. Fluid Mech. **238**, 325 (1992).
[8] M. Lesieur and O. Metais, New trends in large-eddy simulations of turbulence, Annu. Rev. Fluid Mech. **28**, 45 (1996).
[9] C. Meneveau and J. Katz, Scale-invariance and turbulence models for large-eddy simulation, Annu. Rev. Fluid Mech. **32**, 1 (2000).
[10] U. Piomelli, Large-eddy simulation: Achievements and challenges, Prog. Aerospace Sci. **35**, 335 (1999).
[11] T. Bohr, M. H. Jensen, G. Paladin, and A. Vulpiani, *Dynamical Systems Approach to Turbulence* (Cambridge University Press, Cambridge, 2005).
[12] U. Frisch, *Turbulence. The legacy of A. N Kolmogorov* (Cambridge University Press, Cambridge, 1995).
[13] H. Tennekes and J. L. Lumley, *A First Course in Turbulence* (MIT Press, Cambridge, MA, 1990).
[14] R. O. Fox, *Computational Models for Turbulent Reacting Flows* (Cambridge University Press, Cambridge, 2003).
[15] P. Moin and K. Mahesh, Direct numerical simulation: A tool in turbulence research, Annu. Rev. Fluid Mech. **30**, 539 (1998).
[16] W. C. Reynolds, The potential and limitations of direct and large eddy simulations, in *Whither turbulence? Turbulence at the crossroads* (Springer, New York, 1990), pp. 313–343.

[17] A. Alexakis and L. Biferale, Cascades and transitions in turbulent flows, Phys. Rep. **767-769**, 1 (2018).
[18] V. Borue and S. A. Orszag, Local energy flux and subgrid-scale statistics in three-dimensional turbulence, J. Fluid Mech. **366**, 1 (1998).
[19] J. Chen, E. Hawkes, R. Sankaran, S. Mason, and H. Im, Direct numerical simulation of ignition front propagation in a constant volume with temperature inhomogeneities. I. Fundamental analysis and diagnostics, Combust. Flame **145**, 128 (2006).
[20] Q. Chen, S. Chen, and G. L. Eyink, The joint cascade of energy and helicity in three-dimensional turbulence, Phys. Fluids **15**, 361 (2003).
[21] S. Chen, G. L. Eyink, M. Wan, and Z. Xiao, Is the Kelvin theorem valid for high Reynolds number turbulence? Phys. Rev. Lett. **97**, 144505 (2006).
[22] G. L. Eyink and K. R. Sreenivasan, Onsager and the theory of hydrodynamic turbulence, Rev. Mod. Phys. **78**, 87 (2006).
[23] L. Chevillard and C. Meneveau, Lagrangian time correlations of vorticity alignments in isotropic turbulence: Observations and model predictions, Phys. Fluids **23**, 101704 (2011).
[24] L. Chevillard, C. Meneveau, L. Biferale, and F. Toschi, Modeling the pressure Hessian and viscous Laplacian in turbulence: Comparisons with DNS and implications on velocity gradient dynamics, Phys. Fluids **20**, 101504 (2008).
[25] J. Smagorinsky, General circulation experiments with the primitive equations: I. The basic experiment, Month. Weather Rev. **91**, 99 (1963).
[26] A. Misra and D. I. Pullin, A vortex-based subgrid stress model for large-eddy simulation, Phys. Fluids **9**, 2443 (1997).
[27] A. Tsinober, *An Informal Conceptual Introduction to Turbulence* (Springer, New York, 2009).
[28] R. Betchov, An inequality concerning the production of vorticity in isotropic turbulence, J. Fluid Mech. **1**, 497 (1956).
[29] A. Tsinober, Vortex stretching versus production of strain/dissipation, *Turbulence Structure and Vortex Dynamics*, edited by J. C. R Hunt and J. C. Vassilicos (Cambridge University Press, Cambridge, 2000), pp. 164–191.
[30] B. Vreman, B. Geurts, and H. Kuerten, Large-eddy simulation of the turbulent mixing layer, J. Fluid Mech. **339**, 357 (1997).
[31] P. D. Mininni, D. Rosenberg, R. Reddy, and A. Pouquet, A hybrid mpi–openmp scheme for scalable parallel pseudospectral computations for fluid turbulence, Parallel Comput. **37**, 316 (2011).
[32] M. Buzzicotti, M. Linkmann, H. Aluie, L. Biferale, J. Brasseur, and C. Meneveau, Effect of filter type on the statistics of energy transfer between resolved and subfilter scales from *a priori* analysis of direct numerical simulations of isotropic turbulence, J. Turbulence **19**, 167 (2018).
[33] J. A. Domaradzki and D. Carati, A comparison of spectral sharp and smooth filters in the analysis of nonlinear interactions and energy transfer in turbulence, Phys. Fluids **19**, 085111 (2007).
[34] S. Aumaître, S. Fauve, S. McNamara, and P. Poggi, Power injected in dissipative systems and the fluctuation theorem, Europhys. J. B **19**, 449 (2001).
[35] M. Bandi, S. G. Chumakov, and C. Connaughton, Probability distribution of power fluctuations in turbulence, Phys. Rev. E **79**, 016309 (2009).
[36] S. Ciliberto and C. Laroche, An experimental test of the Gallavotti-Cohen fluctuation theorem, J. Phys. IV **08**, Pr6-215 (1998).
[37] D. J. Evans, E. G. D. Cohen, and G. P. Morriss, Probability of second law violations in shearing steady states, Phys. Rev. Lett. **71**, 2401 (1993).
[38] E. Falcon, S. Aumaître, C. Falcón, C. Laroche, and S. Fauve, Fluctuations of energy flux in wave turbulence, Phys. Rev. Lett. **100**, 064503 (2008).
[39] G. Gallavotti and E. G. D. Cohen, Dynamical ensembles in stationary states, J. Stat. Phys. **80**, 931 (1995).
[40] U. M. B. Marconi, A. Puglisi, L. Rondoni, and A. Vulpiani, Fluctuation-dissipation: Response theory in statistical physics, Phys. Rep. **461**, 111 (2008).
[41] X.-D. Shang, P. Tong, and K.-Q. Xia, Test of steady-state fluctuation theorem in turbulent Rayleigh-Bénard convection, Phys. Rev. E **72**, 015301 (2005).

[42] F. Zonta and S. Chibbaro, Entropy production and fluctuation relation in turbulent thermal convection, Europhys. Lett. **114**, 50011 (2016).
[43] H. Aluie and G. L. Eyink, Localness of energy cascade in hydrodynamic turbulence. II. Sharp spectral filter, Phys. Fluids **21**, 115108 (2009).
[44] G. L. Eyink and H. Aluie, Localness of energy cascade in hydrodynamic turbulence. I. Smooth coarse graining, Phys. Fluids **21**, 115107 (2009).
[45] M. Germano, A proposal for a redefinition of the turbulent stresses in the filtered Navier-Stokes equations, Phys. Fluids **29**, 2323 (1986).
[46] C. G. Speziale, Galilean invariance of subgrid-scale stress models in the large-eddy simulation of turbulence, J. Fluid Mech. **156**, 55 (1985).
[47] M. S. Chong, A. E. Perry, and B. J. Cantwell, A general classification of three-dimensional flow fields, Phys. Fluids A **2**, 765 (1990).
[48] A. Ooi, J. Martin, J. Soria, and M. S. Chong, A study of the evolution and characteristics of the invariants of the velocity-gradient tensor in isotropic turbulence, J. Fluid Mech. **381**, 141 (1999).